ELECTRONIC RESEARCH ARCHIVE
Volume **29**, Number **1**, March **2021**

doi:10.3934/era.2020096
pp. **1881–1895**

VISCOSITY ROBUST WEAK GALERKIN FINITE ELEMENT METHODS FOR STOKES PROBLEMS

Bin Wang

Craft & Hawkins Department of Petroleum Engineering
Louisiana State University, 2245 Patrick F Taylor Hall, Baton Rouge, LA, 70803, USA

Lin Mu*

Department of Mathematics
University of Georgia, Athens, GA, 30605, USA

Abstract. In this paper, we develop a viscosity robust weak Galerkin finite element scheme for Stokes equations. The major idea for achieving pressure-independent energy-error estimate is to use a divergence preserving velocity reconstruction operator in the discretization of the right hand side body force. The optimal convergence results for velocity and pressure have been established in this paper. Finally, numerical examples are presented for validating the theoretical conclusions.

1. **Introduction.** In this paper, we consider the following viscosity dependent Stokes equations: Find velocity $\mathbf{u} : \Omega \to \mathbb{R}^d$ ($d = 2$ or 3) and pressure: $p : \Omega \to \mathbb{R}$ such that:

$$-\nu\Delta\mathbf{u} + \nabla p = \mathbf{f}, \text{ in } \Omega, \tag{1}$$

$$\nabla \cdot \mathbf{u} = 0, \text{ in } \Omega, \tag{2}$$

$$\mathbf{u} = 0, \text{ on } \partial\Omega, \tag{3}$$

where $\nu > 0$ is a constant viscosity parameter and $\mathbf{f} \in [L^2(\Omega)]^d$ is a given vector field.

For standard discretizations, one typically has the velocity error measured in H^1-norm as follows:

$$\|\nabla(\mathbf{u}_h - \mathbf{u})\|_h \le C\big(\inf_{\mathbf{w}\in V_h} \|\nabla(\mathbf{u} - \mathbf{w})\|_h + \frac{1}{\nu}\inf_{q\in W_h} \|p - q\|\big),$$

here V_h and W_h denote the finite element space for approximation of velocity and pressure. Besides, $\|\cdot\|_h$ denotes the discrete norm. Thus, if $\nabla \cdot V_h \neq W_h$, the right-hand side shows the dependency of velocity error measured in H^1-norm with respect to the viscosity. Also this dependency may introduce the effect of poor mass conservation for small values in viscosity ν.

Several techniques are proposed in the previous literature for dealing with the above mentioned mass conservation issue. Recently, Linke et al. [5, 6, 7] proposed a

2020 *Mathematics Subject Classification.* Primary: 65N15, 65N30; Secondary: 35B45, 35J50, 35J35.

Key words and phrases. Weak Galerkin, finite element methods, Stokes equations, divergence preserving, pressure robust error estimate.

* Corresponding author: Lin Mu.

class of discretizations, which achieves the pressure robust upper bound via modifying the standard numerical schemes only by revising the right hand side assembling load vectors but remaining the same stiffness matrix. His results are shown as follows:

$$\|\nabla(\mathbf{u}_h - \mathbf{u})\|_h \leq C \inf_{\mathbf{w}\in V_h} \|\nabla(\mathbf{u} - \mathbf{w})\|_h.$$

The key component for developing the pressure-independent scheme is that discrete divergence-free velocity test functions are mapped to exact divergence-free ones by the velocity reconstruction operator. Then the irrotational parts in the load function $\mathbf{f}$ are orthogonal to the mapped discrete-divergence velocity test functions, and thus break the locking phenomena due to the poor mass conservation. Note that similar pressure-robust velocity error estimates can also be achieved with divergence-free mixed methods like [14, 3, 4].

In this paper, we shall apply the velocity reconstruction technique and apply it to the weak Galerkin finite element methods for solving the Stokes equations. Weak Galerkin finite element methods was first proposed by Wang and Ye for solving second order elliptic equations on the polygonal meshes [12]. Recently, this methods have been applied to different partial differential equations, such as [13, 10, 11, 8]. The corresponding velocity reconstruction operators belong to H(div)-conforming finite element spaces and and are defined element-wise. Our scheme shows the feature of in-dependency with respect to pressure. Besides, optimal convergence rate for velocity and pressure have also been established in this paper. The paper is organized as follows. In Section 2, we present the finite element space and numerical scheme. The H(div)-conforming reconstruction is introduced in Section 2.5. Our main results, including stability, error estimates are treated in Section 3. Numerical examples are presented in Section 4 to validate our theoretical conclusions. Finally, the conclusions and future work are summarized in Section 5.

2. Finite element space and numerical scheme.

2.1. **Finite element space.** Let $\mathcal{T}_h$ be a simplicial mesh of the domain Ω. Assume that partition $\mathcal{T}_h$ is shape regular, provided that there exists a number $\tau > 0$ such that $\forall T \in \mathcal{T}_h$ contains a circle of radius ρ_T with $\rho_T \geq \frac{h_T}{\tau}$, where h_T is the diameter of T. Denote mesh size $h := \max h_T$. Denote by $\mathcal{E}_h$ the set of all edges in $\mathcal{T}_h$, and let $\mathcal{E}_h^0 = \mathcal{E}_h \backslash \partial\Omega$ be the set of all interior edges.

We define a weak Galerkin finite element space for the velocity variable as follows:

$$V_h = \{\mathbf{v} = \{\mathbf{v}_0, \mathbf{v}_b\} : \mathbf{v}_0|_T \in [\mathbb{P}_k(T)]^d, \mathbf{v}_b|_e \in [\mathbb{P}_k(e)]^d, e \subset \partial T\},$$

where $k \geq 0$. We emphasize that there is only a *single* value $\mathbf{v}_b$ defined on each edge $e \in \mathcal{E}_h$. For the pressure variable, we define the following finite element space

$$W_h = \{q \in L_0^2(\Omega) : q|_T \in \mathbb{P}_k(T)\},$$

where $L_0^2(\Omega) := \{q : \int_\Omega q d\Omega = 0\}$. Denote by V_h^0 the subspace of V_h consisting of discrete weak functions with vanishing boundary value; i.e.,

$$V_h^0 = \{\mathbf{v} = \{\mathbf{v}_0, \mathbf{v}_b\} \in V_h : \mathbf{v}_b = 0 \text{ on } \partial\Omega\}.$$

Let $[\mathbb{RT}_j(T)]^d$ be a space of Raviart-Thomas element of order j on element T. That is, $\mathbb{RT}_j(T) := [\mathbb{P}_j(T)]^d + \mathbf{x}\mathbb{P}_j(T)$. Here the space $[\mathbb{RT}_k(T)]^{d\times d}$ denotes a space with

each column belongs to $[\mathbb{RT}_k(T)]^d$. The discrete weak gradient (∇_w) and weak divergence $(\nabla_w\cdot)$ for space V_h can be computed on each element T:

$$(\nabla_w \mathbf{v}, \Psi)_T = -(\mathbf{v}_0, \nabla\cdot\Psi)_T + \langle \mathbf{v}_b\cdot\mathbf{n}, \Psi\rangle_{\partial T},\ \forall \Psi \in [\mathbb{RT}_k(T)]^{d\times d}, \tag{4}$$

$$(\nabla_w\cdot\mathbf{v}, \phi)_T = -(\mathbf{v}_0, \nabla\phi) + \langle \mathbf{v}_b\cdot\mathbf{n}, \phi\rangle_{\partial T},\ \forall \phi \in \mathbb{P}_k(T). \tag{5}$$

The usual L^2 inner product can be written locally on each element as follows

$$\begin{aligned}(\nabla_w\mathbf{v}, \nabla_w\mathbf{w}) &= \sum_{T\in\mathcal{T}_h} (\nabla_w\mathbf{v}, \nabla_w\mathbf{w})_T,\\ (\nabla_w\cdot\mathbf{v}, q) &= \sum_{T\in\mathcal{T}_h} (\nabla_w\cdot\mathbf{v}, q)_T.\end{aligned}$$

2.2. **Divergence-preserving velocity reconstruction.** In this section, we shall introduce the divergence preserving velocity reconstruction operator whose normal component at mesh interfaces only depends on the face-based discrete velocities. We denote the following two spaces:

$$\begin{aligned}H(\mathrm{div};\Omega) &= \{\mathbf{w}\in[L^2(\Omega)]^d |\ \mathrm{div}\ \mathbf{w}\in L^2(\Omega)\},\\ H_0(\mathrm{div};\Omega) &= \{\mathbf{w}\in H(\mathrm{div}\,\Omega) |\ \mathbf{v}\cdot\mathbf{n}|_{\partial\Omega}=0\},\end{aligned}$$

where $\mathbf{n}$ denotes the outward unit normal of $\partial\Omega$.

Define the velocity construction operator as $\mathbf{R}_{\mathrm{T}} : V_h \to [\mathbb{RT}_k(T)]^d \subset H_0(\mathrm{div};\Omega)$ such that, for all $\mathbf{v} = \{\mathbf{v}_0, \mathbf{v}_b\} \in V_h$,

$$\int_T \mathbf{R}_{\mathrm{T}}(\mathbf{v})\cdot\mathbf{w}dT = \int_T \mathbf{v}_0\cdot\mathbf{w}dT,\quad \forall \mathbf{w}\in[\mathbb{P}^{k-1}(T)]^d, \tag{6}$$

$$\int_e \mathbf{R}_{\mathrm{T}}(\mathbf{v})\cdot\mathbf{n}qds = \int_e \mathbf{v}_b\cdot\mathbf{n}qds,\quad \forall q\in\mathbb{P}^k(e), e\in\partial T, \tag{7}$$

where it is understood that (6) is not needed in the case of $k = 0$. The major properties of $\mathbf{R}_{\mathrm{T}}$ are summarized in Section 2.5.

2.3. **Numerical scheme.** We first introduce two bilinear forms as follows

$$\begin{aligned}a(\mathbf{v},\mathbf{w}) &= \nu(\nabla_w\mathbf{v}, \nabla_w\mathbf{w}),\\ b(\mathbf{v}, q) &= (\nabla_w\cdot\mathbf{v}, q).\end{aligned}$$

We are now ready to describe our new weak Galerkin finite element scheme for the Stokes equations (1)-(3) as algorithm 2.1.

Algorithm 2.1. (New WG Algorithm) A numerical approximation for (1)-(3) is to find $\mathbf{u}_h = \{\mathbf{u}_0, \mathbf{u}_b\} \in V_h^0$ and $p_h \in W_h$ such that

$$a(\mathbf{u}_h,\mathbf{v}) - b(\mathbf{v}, p_h) = (\mathbf{f}, \mathbf{R}_{\mathrm{T}}(\mathbf{v})), \tag{8}$$

$$b(\mathbf{u}_h, q) = 0, \tag{9}$$

for all $\mathbf{v} = \{\mathbf{v}_0, \mathbf{v}_b\} \in V_h^0$ and $q \in W_h$. Here $\mathbf{R}_{\mathrm{T}}(\mathbf{v})$ is defined in (6)-(7).

In the following, the standard scheme [13] as Algorithm 2.2 will be also cited for comparison.

Algorithm 2.2. (Standard WG Algorithm) A numerical approximation for (1)-(3) is to find $\mathbf{u}_h = \{\mathbf{u}_0, \mathbf{u}_b\} \in V_h^0$ and $p_h \in W_h$ such that

$$a(\mathbf{u}_h,\mathbf{v}) - b(\mathbf{v}, p_h) = (\mathbf{f}, \mathbf{v}_0), \tag{10}$$

$$b(\mathbf{u}_h, q) = 0, \tag{11}$$

for all $\mathbf{v} = \{\mathbf{v}_0, \mathbf{v}_b\} \in V_h^0$ and $q \in W_h$.

Remark 1. The Algorithm 2.1 and Algorithm 2.2 share the same stiffness matrix but only differ at the right hand side.

In the following, C denotes a generic constant independent of the mesh size h and the functions in the estimates. The notation of $a \lesssim b$ will be employed with the meaning $a \leq Cb$.

2.4. **Preliminary results.** We introduce the following discrete norms on V_h:

$$|||\mathbf{v}|||^2 := \sum_{T\in\mathcal{T}_h} \|\nabla_w \mathbf{v}\|_T^2, \text{ and } |||\mathbf{v}|||_T^2 := \|\nabla_w \mathbf{v}\|_T^2. \tag{12}$$

Besides, we also denote:

$$\|\mathbf{v}\|_{1,h}^2 := \sum_{T\in\mathcal{T}_h} \left(\|\nabla \mathbf{v}_0\|_T^2 + h_T^{-1} \|\mathbf{v}_0 - \mathbf{v}_b\|_{\partial T}^2 \right).$$

As shown in [9], the defined $|||\cdot|||$-norm is a norm in V_h^0. We cite the following lemmas.

Lemma 2.3. *For any $\mathbf{v} = \{\mathbf{v}_0, \mathbf{v}_b\} \in V_h$, we have the following equivalence between the two norms:*

$$C_1 \|\mathbf{v}\|_{1,h} \leq |||\mathbf{v}||| \leq C_2 \|\mathbf{v}\|_{1,h}.$$

Lemma 2.4. *For any $\mathbf{v}, \mathbf{w} \in V_h^0$, we have*[9]

$$|a(\mathbf{v}, \mathbf{w})| \leq \nu |||\mathbf{v}||| |||\mathbf{w}|||, \tag{13}$$

$$a(\mathbf{v}, \mathbf{v}) = \nu |||\mathbf{v}|||^2. \tag{14}$$

Denote by $\boldsymbol{\pi}_h$ as a projection such that $\boldsymbol{\pi}_h \mathbf{q} \in [H(\mathrm{div}, \Omega)]^d$ for $\mathbf{q} \in [H(\mathrm{div}, \Omega)]^d$, and on each $T \in \mathcal{T}_h$, one has $\boldsymbol{\pi}_h \mathbf{q} \in [\mathbb{RT}_k(T)]^d$ and the following equation is satisfied:

$$(\nabla \cdot \mathbf{q}, \mathbf{v}_0)_T = (\nabla \cdot \boldsymbol{\pi}_h \mathbf{q}, \mathbf{v}_0)_T, \ \forall \mathbf{v}_0 \in [\mathbb{P}_k(T)]^d.$$

For any $\boldsymbol{\tau} \in [H(\mathrm{div}, \Omega)]^d$, we have

$$\sum_{T\in\mathcal{T}_h} (-\nabla \cdot \boldsymbol{\tau}, \mathbf{v}_0)_T = \sum_{T\in\mathcal{T}_h} (\boldsymbol{\pi}_h \boldsymbol{\tau}, \nabla_w \mathbf{v})_T, \ \forall \mathbf{v} = \{\mathbf{v}_0, \mathbf{v}_b\} \in V_h. \tag{15}$$

Besides, we also define $\tilde{\boldsymbol{\pi}}_h$ as a L^2 projection from $[L^2(T)]^{d\times d}$ to $[\mathbb{RT}_k(T)]^{d\times d}$.

Denote The L^2-projection in the finite element space V_h is given by $\mathbf{Q}_h \mathbf{v} = \{\mathbf{Q}_0 \mathbf{v}, \mathbf{Q}_b \mathbf{v}\}$ for $\mathbf{v} \in [H^1(\Omega)]^d$. Similarly, denote the L^2-projection into piece-wise finite element space $\mathbb{P}_\ell(T)$ by Π_h^ℓ. When $\ell = k$, we will denote the projection operator Π_h^k by Π_h. Thus, Π_h denotes the projection to the finite element space W_h.

Lemma 2.5. *The projection operators $\mathbf{Q}_h$, $\tilde{\boldsymbol{\pi}}_h$, and Π_h satisfy the following commutative properties:*[9]

$$\nabla_w (\mathbf{Q}_h \mathbf{v}) = \tilde{\boldsymbol{\pi}}_h (\nabla \mathbf{v}), \quad \forall \mathbf{v} \in [H^1(\Omega)]^d, \tag{16}$$

$$\nabla_w \cdot (\mathbf{Q}_h \mathbf{v}) = \Pi_h (\nabla \cdot \mathbf{v}), \quad \forall \mathbf{v} \in H(div; \Omega). \tag{17}$$

Lemma 2.6. *There exists a positive constant β, which is independent of h such that*[13]

$$\sup_{\mathbf{v}\in V_h^0} \frac{b(\mathbf{v}, \rho)}{|||\mathbf{v}|||} \geq \beta \|\rho\|, \tag{18}$$

for all $\rho \in W_h$.

Thus, we have the following theorem.

Theorem 2.7. *The weak Galerkin finite element Algorithm 2.1 and 2.2 admit one and only one solution.*

Lemma 2.8. *Let $\mathcal{T}_h$ be a finite element partition of Ω satisfying the shape regularity assumptions and $\mathbf{w} \in [H^{r+1}(\Omega)]^d$ and $\rho \in H^r(\Omega)$ with $1 \le r \le k$. Then, for $0 \le s \le 1$, we have* [9]

$$\sum_{T\in\mathcal{T}_h} h_T^{2s}\|\mathbf{w}-\mathbf{Q}_0\mathbf{w}\|_{T,s}^2 \lesssim h^{2(r+1)}\|\mathbf{w}\|_{r+1}^2, \tag{19}$$

$$\sum_{T\in\mathcal{T}_h} h_T^{2s}\|\nabla\mathbf{w}-\tilde{\pi}_h(\nabla\mathbf{w})\|_{T,s}^2 \lesssim h^{2(r)}\|\mathbf{w}\|_{r+1}^2, \tag{20}$$

$$\sum_{T\in\mathcal{T}_h} h_T^{2s}\|\rho-\Pi_h\rho\|_{T,s}^2 \lesssim h^{2(r)}\|\rho\|_r^2. \tag{21}$$

Let T be an element with e as an edge. For any function $g \in H^1(T)$, the following trace inequality has been proved to be valid for general meshes satisfying the shape regular assumptions:

$$\|g\|_e^2 \le C\left(h_T^{-1}\|g\|_T^2 + h_T\|\nabla g\|_T^2\right). \tag{22}$$

Lemma 2.9. *For any $\mathbf{v} = \{\mathbf{v}_0, \mathbf{v}_b\} \in V_h$, we have*[9]

$$\sum_{T\in\mathcal{T}_h} \|\nabla\mathbf{v}_0\|_T^2 \lesssim |\!|\!|\mathbf{v}|\!|\!|^2. \tag{23}$$

2.5. **Properties of velocity reconstruction operator.** In this section, we shall review the $H(\mathrm{div})$-conforming reconstruction operator for later use. Denote $\mathbb{\Pi}_T$ as a projection to $[\mathbb{RT}_k(T)]^d$.

Lemma 2.10. *The operator $\mathbf{R}_T$ is divergence-preserving, i.e., for all $\mathbf{v} \in V_h$, the following holds:*

$$\mathrm{div}(\mathbf{R}_T(\mathbf{v})) = \nabla_w \cdot \mathbf{v}, \tag{24}$$

and $\mathbf{R}_T(\mathbf{v})|_e \cdot \mathbf{n}$ only depends on $\mathbf{v}_b|_e \cdot \mathbf{n}$. Besides, for all $\mathbf{v} \in V_h$, the following bound holds:

$$\|\mathbf{R}_T(\mathbf{v}) - \mathbf{v}_0\|_T \lesssim \sum_{e\in\partial T} h_e^{1/2}\|(\mathbf{v}_0-\mathbf{v}_b)\cdot\mathbf{n}\|_e. \tag{25}$$

Proof. For all $q \in \mathbb{P}_k(T)$, by using integration by parts, the definition of $\mathbf{R}_T(\mathbf{v})$ as (6)-(7), and the definition of $\nabla_w \cdot \mathbf{v}$ in (5), we arrive at

$$\begin{aligned}(\mathrm{div}(\mathbf{R}_T(\mathbf{v})), q)_T &= -(\mathbf{R}_T(\mathbf{v}), \nabla q)_T + \langle \mathbf{R}_T(\mathbf{v})\cdot\mathbf{n}, q\rangle_{\partial T}\\ &= -(\mathbf{v}_0, \nabla q)_T + \langle \mathbf{v}_b\cdot\mathbf{n}, q\rangle_{\partial T}\\ &= (\nabla_w\cdot\mathbf{v}, q)_T,\end{aligned}$$

and thus proves (24).

Since $[\mathbb{P}_k(T)]^2 \in [\mathbb{RT}_k(T)]^2$, we have $\mathbb{\Pi}_T(\mathbf{v}_0) = \mathbf{v}_0$. By triangle inequality, Cauchy-Schwartz inequality, it is obtained,

$$\begin{aligned}\|\mathbf{v}_0 - \mathbf{R}_T(\mathbf{v})\|_T^2 &= \|\mathbb{\Pi}_T(\mathbf{v}_0) - \mathbf{R}_T(\mathbf{v})\|_T^2\\ &\lesssim \sum_{e\in\partial T} h_e\|(\mathbf{v}_0-\mathbf{v}_b)\cdot\mathbf{n}\|_e^2.\end{aligned}$$

Here we have applied the inequality $\|\Theta\|_T \lesssim (\|\Pi_h^{k-1}\Theta\|_T^2 + \sum_{e\in\partial T} h_e\|\Theta\cdot\mathbf{n}\|_e^2)^{1/2}$ for $\Theta \in [\mathbb{RT}_k(T)]^d$ and $\Theta = \mathbb{\Pi}_T(\mathbf{v}_0) - \mathbf{R}_{\mathrm{T}}(\mathbf{v})$, $\Pi_h^{k-1}(\mathbb{\Pi}_T(\mathbf{v}_0) - \mathbf{R}_{\mathrm{T}}(\mathbf{v})) = 0$ in the last step. Thus the above completes the proof. □

3. Main results.

In this section, we shall present the main results concerning the convergence analysis of scheme (8)-(9).

3.1. Error equation.

Denote by $\mathbf{u}$ and p the exact solution of (1)-(3). Denote by $\mathbf{e}_h$ and ϵ_h the corresponding error given by

$$\mathbf{e}_h = \{\mathbf{e}_0, \mathbf{e}_b\} = \{\mathbf{Q}_0\mathbf{u} - \mathbf{u}_0, \mathbf{Q}_b\mathbf{u} - \mathbf{u}_b\}, \quad \epsilon_h = \Pi_h p - p_h. \tag{26}$$

Lemma 3.1. *Let $(\mathbf{w};\rho) \in [H^1(\Omega)]^d \times L^2(\Omega)$ be sufficiently smooth and satisfy the following equation*

$$-\nu\Delta\mathbf{w} + \nabla\rho = \eta, \tag{27}$$

in the domain Ω. Let $\mathbf{Q}_h\mathbf{w} = \{\mathbf{Q}_0\mathbf{w}, \mathbf{Q}_b\mathbf{w}\}$ and $\Pi_h\rho$ be the L^2-projection of $(\mathbf{w};\rho)$ into the finite element space $V_h \times W_h$. Then, the following equation holds

$$(\nu\nabla_w(\mathbf{Q}_h\mathbf{w}), \nabla_w\mathbf{v}) - (\nabla_w\cdot\mathbf{v}, \Pi_h\rho) = (\eta, \mathbf{R}_T(\mathbf{v})) + \nu\ell_{\mathbf{w}}(\mathbf{v}) + D_{\mathbf{w}}(\mathbf{v}), \tag{28}$$

for all $\mathbf{v} \in V_h^0$, where $\ell_{\mathbf{w}}$ and $D_{\mathbf{w}}$ are defined by

$$\ell_{\mathbf{w}}(\mathbf{v}) = \sum_{T\in\mathcal{T}_h} (\boldsymbol{\pi}_h\nabla\mathbf{w} - \tilde{\boldsymbol{\pi}}_h\nabla\mathbf{w}, \nabla_w\mathbf{v})_T, \tag{29}$$

$$D_{\mathbf{w}}(\mathbf{v}) = \sum_{T\in\mathcal{T}_h} (\nu\Delta\mathbf{w}, \mathbf{v}_0 - \mathbf{R}_T(\mathbf{v}))_T. \tag{30}$$

Proof. Test (27) by $\mathbf{R}_{\mathrm{T}}(\mathbf{v})$ to obtain:

$$\begin{aligned}(\eta, \mathbf{R}_{\mathrm{T}}(\mathbf{v})) &= -(\nu\Delta\mathbf{w}, \mathbf{R}_{\mathrm{T}}(\mathbf{v})) + (\nabla\rho, \mathbf{R}_{\mathrm{T}}(\mathbf{v}))\\ &= -(\nu\Delta\mathbf{w}, \mathbf{v}_0) + (\nu\Delta\mathbf{w}, \mathbf{v}_0 - \mathbf{R}_{\mathrm{T}}(\mathbf{v})) + (\nabla\rho, \mathbf{R}_{\mathrm{T}}(\mathbf{v}))\\ &= \nu I_1 + I_2 + I_3.\end{aligned} \tag{31}$$

It follows from the integration by parts, definition of $\boldsymbol{\pi}_h$, and definition of ∇_w that

$$\begin{aligned}I_1 &= -(\Delta\mathbf{w}, \mathbf{v}_0) = -(\nabla\cdot\nabla\mathbf{w}, \mathbf{v}_0) = (\boldsymbol{\pi}_h(\nabla\mathbf{w}), \nabla_w\mathbf{v})\\ &= (\nabla_w\mathbf{Q}_h\mathbf{w}, \nabla_w\mathbf{v}) + (\boldsymbol{\pi}_h(\nabla\mathbf{w}) - \nabla_w\mathbf{Q}_h\mathbf{w}, \nabla_w\mathbf{v})\\ &= (\nabla_w\mathbf{Q}_h\mathbf{w}, \nabla_w\mathbf{v}) + (\boldsymbol{\pi}_h(\nabla\mathbf{w}) - \tilde{\boldsymbol{\pi}}_h(\nabla\mathbf{w}), \nabla_w\mathbf{v}).\end{aligned}$$

For the second term, we have

$$I_2 = \sum_{T\in\mathcal{T}_h} (\nu\Delta\mathbf{w}, \mathbf{v}_0 - \mathbf{R}_{\mathrm{T}}(\mathbf{v}))_T := D_{\mathbf{w}}(\mathbf{v}).$$

By integration by parts, $\mathbf{R}_{\mathrm{T}}(\mathbf{v})$ has continuous normal component at mesh interfaces and ρ is continuous across interfaces, and the property of $\nabla\cdot\mathbf{R}_{\mathrm{T}}(\mathbf{v})$, it follows,

$$\begin{aligned}I_3 &= (\nabla\rho, \mathbf{R}_{\mathrm{T}}(\mathbf{v})) = \sum_{T\in\mathcal{T}_h} -(\rho, \nabla\cdot\mathbf{R}_{\mathrm{T}}(\mathbf{v}))_T + \langle\rho, \mathbf{R}_{\mathrm{T}}(\mathbf{v})\cdot\mathbf{n}\rangle_{\partial T}\\ &= \sum_{T\in\mathcal{T}_h} -(\Pi_h\rho, \nabla\cdot\mathbf{R}_{\mathrm{T}}(\mathbf{v}))_T = -(\Pi_h\rho, \nabla_w\cdot\mathbf{v}).\end{aligned}$$

Here we have used (24) in the last step. By substituting all terms I_1, I_2, I_3 into (31), we complete the proof. □

The following is a result on the error equation for the weak Galerkin finite element scheme.

Lemma 3.2. *Let $\mathbf{e}_h$ and ϵ_h be the errors of the weak Galerkin finite element solutions arising from (8)-(9), then we have*

$$a(\mathbf{e}_h, \mathbf{v}) - b(\mathbf{v}, \epsilon_h) = \psi_{\mathbf{u}}(\mathbf{v}), \tag{32}$$

$$b(\mathbf{e}_h, q) = 0, \tag{33}$$

for all $\mathbf{v} \in V_h^0$ and $q \in W_h$, where $\psi_{\mathbf{u}}(\mathbf{v}) = \nu \ell_{\mathbf{u}}(\mathbf{v}) + D_{\mathbf{u}}(\mathbf{v})$ is a linear functional defined on V_h^0.

Proof. Since $\mathbf{u}$ and p satisfies (27) with $\eta = \mathbf{f}$, then from (28) we have

$$(\nu \nabla_w(\mathbf{Q}_h \mathbf{u}), \nabla_w \mathbf{v}) - (\nabla_w \cdot \mathbf{v}, \Pi_h p) = (\mathbf{f}, \mathbf{R}_{\mathrm{T}}(\mathbf{v})) + \nu \ell_{\mathbf{u}}(\mathbf{v}) + D_{\mathbf{u}}(\mathbf{v}).$$

The above equation gives,

$$a(\mathbf{Q}_h \mathbf{u}, \mathbf{v}) - b(\mathbf{v}, \Pi_h p) = (\mathbf{f}, \mathbf{R}_{\mathrm{T}}(\mathbf{v})) + \nu \ell_{\mathbf{u}}(\mathbf{v}) + D_{\mathbf{u}}(\mathbf{v}).$$

The difference of above equation and (8) gives the following equation,

$$a(\mathbf{e}_h, \mathbf{v}) - b(\mathbf{v}, \epsilon_h) = \nu \ell_{\mathbf{u}}(\mathbf{v}) + D_{\mathbf{u}}(\mathbf{v}) \tag{34}$$

for all $\mathbf{v} \in V_h^0$ and thus completes (32).

Then, we test (2) by $q \in W_h$ and use Lemma 2.5 to obtain

$$0 = (\nabla \cdot \mathbf{u}, q) = (\nabla_w \cdot \mathbf{Q}_h \mathbf{u}, q). \tag{35}$$

The difference between above equation and (9) yields the following:

$$b(\mathbf{e}_h, q) = 0,$$

for all $q \in W_h$. Thus, we complete the proof. □

Lemma 3.3. *Assume the finite element partition $\mathcal{T}_h$ is shape regular and $\mathbf{w} \in [H^{k+2}(\Omega)]^d$, we have following estimates true for $\mathbf{v} \in V_h$:*

$$|\ell_{\mathbf{w}}(\mathbf{v})| \lesssim h^{k+1} \|\mathbf{w}\|_{k+2} |||\mathbf{v}|||, \tag{36}$$

$$|D_{\mathbf{w}}(\mathbf{v})| \lesssim \nu h^{k+1} \|\mathbf{w}\|_{k+2} |||\mathbf{v}|||. \tag{37}$$

Proof. (36) can be found in [9]. By Cauchy-Schwartz inequality, and estimate (25), it implies:

$$\begin{aligned} D_{\mathbf{w}}(\mathbf{v}) &= (\nu \Delta \mathbf{w}, \mathbf{v}_0 - \mathbf{R}_{\mathrm{T}}(\mathbf{v})) \\ &= \nu(\Delta \mathbf{w} - \Pi_h^{k-1}(\Delta \mathbf{w}), \mathbf{v}_0 - \mathbf{R}_{\mathrm{T}}(\mathbf{v})) \\ &\leq \nu h^k \|\mathbf{w}\|_{k+2} \Big(\sum_{T \in \mathcal{T}_h} h \|\mathbf{v}_0 - \mathbf{v}_b\|_{\partial T}^2 \Big)^{1/2} \\ &\lesssim \nu h^{k+1} \|\mathbf{w}\|_{k+2} |||\mathbf{v}|||. \end{aligned}$$

Thus, we complete the proof. □

3.2. **Error estimates.** In this section, we shall establish optimal order error estimates for the velocity approximation $\mathbf{u}_h$ in a $|||\cdot|||$-norm and L^2-norm, and for the pressure approximation p_h in the standard L^2-norm.

Theorem 3.4. *Let $(\mathbf{u},p)\in[H_0^1(\Omega)]^d\times L_0^2(\Omega)$ and $(\mathbf{u}_h,p_h)\in V_h^0\times W_h$ denote the unique solutions of equations (1)-(3) and (8)-(9), respectively, and assume the additional regularity $\mathbf{u}\in[H^{k+2}(\Omega)]^d$. Then the following estimates hold:*

$$|||\mathbf{Q}_h\mathbf{u}-\mathbf{u}_h||| \lesssim h^{k+1}\|\mathbf{u}\|_{k+2} \tag{38}$$

$$\|\Pi_h p-p_h\| \lesssim \nu h^{k+1}\|\mathbf{u}\|_{k+2}. \tag{39}$$

Proof. Recall $\mathbf{e}_h=\{\mathbf{Q}_0\mathbf{u}-\mathbf{u}_0,\mathbf{Q}_b\mathbf{u}-\mathbf{u}_b\}$ and $\epsilon_h=\Pi_h p-p_h$. By letting $\mathbf{v}=\mathbf{e}_h$ in (32) and $q=\epsilon_h$ in (33) and adding the two resulting equations, plugging in (36)-(37), we obtain:

$$\begin{aligned}\nu|||\mathbf{e}_h|||^2 &= \psi_{\mathbf{u}}(\mathbf{e}_h)\\ &= \nu\ell_{\mathbf{u}}(\mathbf{e}_h)+D_{\mathbf{u}}(\mathbf{e}_h)\\ &\lesssim \nu h^{k+1}\|\mathbf{u}\|_{k+2}|||\mathbf{e}_h|||,\end{aligned}$$

which gives (38). Error equation (32) implies,

$$b(\mathbf{v},\epsilon_h)=a(\mathbf{e}_h,\mathbf{v})-\psi_{\mathbf{u}}(\mathbf{v}).$$

By combining (13), (38), definition of $\psi_{\mathbf{u}}(\mathbf{v})$, estimates in (36)-(37), we arrive at

$$|b(\mathbf{v},\epsilon_h)|\le C\nu h^{k+1}\Big(\|\mathbf{u}\|_{k+2}\Big)|||\mathbf{v}|||,$$

and then together with inf-sup condition,

$$\|\epsilon_h\|\lesssim \nu h^{k+1}\|\mathbf{u}\|_{k+2}.$$

The above completes the proof. □

Remark 2. Furthermore, if under the additional regularity assumption $p\in H^{k+1}(\Omega)$, we have the following bound for the pressure error:

$$\|p_h-p\|\lesssim \nu h^{k+1}\|\mathbf{u}\|_{k+2}+h^{k+1}\|p\|_{k+1}. \tag{40}$$

Remark 3. The error analysis results for Algorithm 2.2 show the following bound if $\mathbf{u}\in[H^{k+2}(\Omega)]^d$, $p\in H^{k+1}(\Omega)$:

$$|||\mathbf{Q}_h\mathbf{u}-\mathbf{u}_h|||\lesssim h^{k+1}\Big(\|\mathbf{u}\|_{k+2}+\frac{1}{\nu}\|p\|_{k+1}\Big). \tag{41}$$

The term $\nu^{-1}\|p\|_{k+1}$ in the right-hand side grows unboundedly as $\nu\to 0^+$, therefore break the accuracy of the velocity approximation.

In the following section, we shall prove the optimal convergence rate of velocity error measured in L^2-norm, which is also viscosity independent.

Theorem 3.5. *Under the assumptions of above theorem, the above elliptic regularity assumption, and $\mathbf{f}\in[H^{k+1}(\Omega)]^d$, the following error estimate holds:*

$$\|\mathbf{Q}_0\mathbf{u}-\mathbf{u}_0\|\lesssim h^{k+2}\big(\|\mathbf{u}\|_{k+2}+\|\mathbf{f}\|_{k+1}\big). \tag{42}$$

Proof. Consider the problem of seeking $(\mathbf{z};\theta)$ such that:

$$\begin{aligned}-\nu\Delta\mathbf{z}+\nabla\theta &= \mathbf{Q}_0\mathbf{u}-\mathbf{u}_0,\ \text{in }\Omega\\ \nabla\cdot\mathbf{z} &= 0,\ \text{in }\Omega\\ \mathbf{z} &= 0,\ \text{on }\partial\Omega.\end{aligned} \tag{43}$$

Assume the dual problem has the $[H^2(\Omega)]^d \times H^1(\Omega)$-regularity property in the sense that the solution $(\mathbf{z};\theta) \in [H^2(\Omega)]^d \times H^1(\Omega)$ and the following a priori estimate holds:

$$\|\mathbf{z}\|_2 + \|\theta\|_1 \lesssim \|\mathbf{Q}_0\mathbf{u} - \mathbf{u}_0\|. \tag{44}$$

Test the first equation of (43) by $\mathbf{e}_0$, by using (15), error equation (33), we have the following:

$$\begin{aligned}
\|\mathbf{e}_0\|^2 &= (-\nu\Delta\mathbf{z}, \mathbf{e}_0) + (\nabla\theta, \mathbf{e}_0) \\
&= -\nu(\nabla\cdot\nabla\mathbf{z}, \mathbf{e}_0) - (\nabla_w\cdot\mathbf{e}_h, \Pi_h\theta) + \langle(\mathbf{e}_0 - \mathbf{e}_b)\cdot\mathbf{n}, (\theta - \Pi_h\theta)\rangle \\
&= \nu(\pi_h(\nabla\mathbf{z}), \nabla_w\mathbf{e}_h) + \langle(\mathbf{e}_0 - \mathbf{e}_b)\cdot\mathbf{n}, (\theta - \Pi_h\theta)\rangle.
\end{aligned}$$

In the following, we shall estimate the terms on the right hand side of the above equation.

Using (16), the definitions of $\tilde{\boldsymbol{\pi}}_h$ and $\mathbf{Q}_0$, the fact $\nu(\nabla\mathbf{u}, \nabla\mathbf{z}) - (\nabla\cdot\mathbf{z}, p) = \nu(\nabla\mathbf{u}, \nabla\mathbf{z}) = (\mathbf{f}, \mathbf{z})$, and using $\nabla_w\cdot\mathbf{u}_h = 0$ in Algorithm 2.1, we have

$$\begin{aligned}
&\left|\sum_T (\nu\nabla\mathbf{z}, \nabla_w\mathbf{e}_h)_T\right| \\
=\ &\left|\sum_T \left((\nu\nabla\mathbf{z}, \nabla_w\mathbf{Q}_h\mathbf{u})_T - (\nu\nabla\mathbf{z}, \nabla_w\mathbf{u}_h)_T\right)\right| \\
=\ &\left|\sum_T \left(\left(\nu\nabla\mathbf{z}, \tilde{\boldsymbol{\pi}}_h(\nabla\mathbf{u})\right)_T - (\nu\nabla\mathbf{z}, \nabla_w\mathbf{u}_h)_T\right)\right| \\
=\ &\left|\sum_T \left(\left(\nu\nabla\mathbf{z}, \tilde{\boldsymbol{\pi}}_h(\nabla\mathbf{u}) - \nabla\mathbf{u}\right)_T + (\nu\nabla\mathbf{z}, \nabla\mathbf{u})_T - (\nu\nabla\mathbf{z}, \nabla_w\mathbf{u}_h)_T\right)\right| \\
=\ &\left|\sum_T \left(\left(\nu\nabla\mathbf{z} - \tilde{\boldsymbol{\pi}}_h(\nabla\mathbf{z})_T, \tilde{\boldsymbol{\pi}}_h(\nabla\mathbf{u}) - \nabla\mathbf{u}\right)_T + (\nu\nabla\mathbf{z}, \nabla\mathbf{u})_T - (\nu\nabla\mathbf{z}, \nabla_w\mathbf{u}_h)_T\right)\right| \\
=\ &\left|\sum_T \left(\left(\nu\nabla\mathbf{z} - \tilde{\boldsymbol{\pi}}_h(\nabla\mathbf{z})_T, \tilde{\boldsymbol{\pi}}_h(\nabla\mathbf{u}) - \nabla\mathbf{u}\right)_T + (\nu\nabla\mathbf{z}, \nabla\mathbf{u})_T - (\nu\nabla_w\mathbf{Q}_h\mathbf{z}, \nabla_w\mathbf{u}_h)_T\right)\right| \\
=\ &\left|\sum_T \left(\left(\nu\nabla\mathbf{z} - \tilde{\boldsymbol{\pi}}_h(\nabla\mathbf{z})_T, \tilde{\boldsymbol{\pi}}_h(\nabla\mathbf{u}) - \nabla\mathbf{u}\right)_T + (\mathbf{f}, \mathbf{z} - \mathbf{R}_T(\mathbf{Q}_h\mathbf{z}))_T\right)\right| \\
=\ &\left|\sum_T \left(\left(\nu\nabla\mathbf{z} - \tilde{\boldsymbol{\pi}}_h(\nabla\mathbf{z})_T, \tilde{\boldsymbol{\pi}}_h(\nabla\mathbf{u}) - \nabla\mathbf{u}\right)_T + (\mathbf{f} - \mathbf{Q}_0\mathbf{f}, \mathbf{z} - \mathbf{R}_T(\mathbf{Q}_h\mathbf{z}))_T\right)\right| \\
\le\ &Ch\nu\|\mathbf{z}\|_2 h^{k+1}\|\mathbf{u}\|_{k+2} + Ch^{k+1}\|\mathbf{f}\|_{k+1} h\|\mathbf{z}\|_1 \\
\le\ &Ch^{k+2}(\nu\|\mathbf{z}\|_2 + \|\mathbf{z}\|_1)\Big(\|\mathbf{u}\|_{k+2} + \|\mathbf{f}\|_{k+1}\Big) \\
\le\ &Ch^{k+2}\|\mathbf{z}\|_2\Big(\|\mathbf{u}\|_{k+2} + \|\mathbf{f}\|_{k+1}\Big).
\end{aligned}$$

The above inequality and (38) imply the following:

$$\begin{aligned}
|\nu(\boldsymbol{\pi}_h(\nabla\mathbf{z}), \nabla_w\mathbf{e}_h)| &= |(\nu\boldsymbol{\pi}_h(\nabla\mathbf{z}) - \nabla\mathbf{z}, \nabla_w\mathbf{e}_h) + (\nu\nabla\mathbf{z}, \nabla_w\mathbf{e}_h)| \\
&\le Ch\nu\|\mathbf{z}\|_2|||\mathbf{e}_h||| + Ch^{k+2}\|\mathbf{z}\|_2(\|\mathbf{u}\|_{k+2} + \|\mathbf{f}\|_{k+1}) \\
&\le Ch^{k+2}\|\mathbf{z}\|_2\big(\|\mathbf{u}\|_{k+2} + \|\mathbf{f}\|_{k+1}\big).
\end{aligned}$$

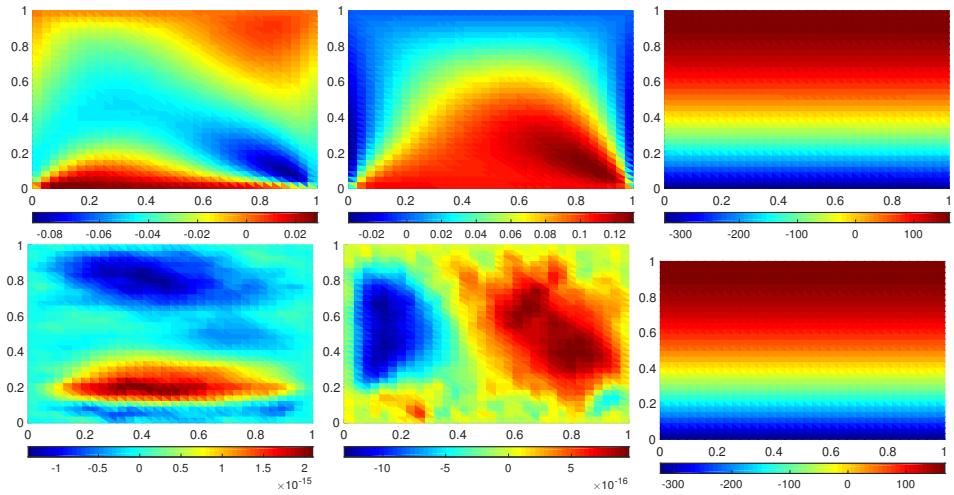

FIGURE 1. Example 4.1: solution from Algorithm 2.2 (top); Algorithm 2.1 (bottom).

Furthermore, by Cauchy-Schwartz inequality, definition of $\|\cdot\|_{1,h}$-norm, (21), and Lemma 2.3, the following holds:

$$\begin{aligned}\langle(\mathbf{e}_0-\mathbf{e}_b)\cdot\mathbf{n},\theta-\Pi_h\theta\rangle &\leq C\sum_{T\in\mathcal{T}_h}\big(h^{-1/2}\|\mathbf{e}_0-\mathbf{e}_b\|_e\big)\big(h^{1/2}\|\theta-\Pi_h\theta\|_{\partial T}\big)\\ &\leq Ch\|\mathbf{e}_h\|_{1,h}\|\theta\|_1\\ &\leq Ch^{k+2}\|\mathbf{u}\|_{k+2}\|\theta\|_1.\end{aligned}$$

Thus, by summing all the above inequality together, we arrive at

$$\begin{aligned}\|\mathbf{e}_0\|^2 &\leq Ch^{k+2}\Big(\|\mathbf{z}\|_2+\|\theta\|_1\Big)\Big(\|\mathbf{u}\|_{k+2}+\|\mathbf{f}\|_{k+1}\Big)\\ &\leq Ch^{k+2}\|\mathbf{e}_0\|\Big(\|\mathbf{u}\|_{k+2}+\|\mathbf{f}\|_{k+1}\Big),\end{aligned}$$

which completes the proof. □

4. **Numerical results.** In this section, several numerical examples in 2D are presented to validate the theoretical results. When the exact solutions have the regularity required by Theorem 3.4, we expect:

- If $(\mathbf{u}_h;p_h)$ are solutions from Algorithm 2.1 (denoted as WG 1):
  - $|||\mathbf{Q}_h\mathbf{u}-\mathbf{u}_h||| \leq Ch^{k+1}\|\mathbf{u}\|_{k+2}$,
  - $\|\mathbf{Q}_0\mathbf{u}-\mathbf{u}_0\| \leq Ch^{k+2}\|\mathbf{u}\|_{k+2}$,
  - $\|\Pi_h p-p_h\| \leq C\nu h^{k+1}\|\mathbf{u}\|_{k+2}$,
- If $(\mathbf{u}_h;p_h)$ are solutions from Algorithm 2.2 (denoted as WG 2):
  - $|||\mathbf{Q}_h\mathbf{u}-\mathbf{u}_h||| \leq Ch^{k+1}(\|\mathbf{u}\|_{k+2}+\nu^{-1}\|p\|_{k+1})$,
  - $\|\mathbf{Q}_0\mathbf{u}-\mathbf{u}_0\| \leq Ch^{k+2}(\|\mathbf{u}\|_{k+2}+\nu^{-1}\|p\|_{k+1})$,
  - $\|\Pi_h p-p_h\| \leq Ch^{k+1}(\nu\|\mathbf{u}\|_{k+2}+\|p\|_{k+1})$.

4.1. **Test 1 (Zero flow).** Let $\Omega = (0,1)^2$, and the exact solutions are chosen as follows:

$$\mathbf{u} = 0,\ p = -\frac{Ra}{2}y^2 + Ra\ y - \frac{Ra}{3},$$

with $Ra = 1000$. Dirichlet boundary condition has been chosen for the test. It is noted that the velocity is chosen as zero for this test. We expect our numerical solution can produce zero solutions for velocity. However, this is not true for the standard numerical scheme. Numerical analysis for Algorithm 2.2 shows that:

$$|||\mathbf{e}_h||| \leq Ch^{k+1}(\|\mathbf{u}\|_{k+2} + \nu^{-1}\|p\|_1),$$

and thus even the problem with zero velocity will deliver a non-zero numerical solution in velocity due to the term of pressure. Different with Algorithm 2.2, the simulation by Algorithm 2.1 will produce a solution in velocity independent of pressure, and we can expect a zero simulation of velocity.

We perform WG simulation (by Algorithm 2.1 and Algorithm 2.2) on $N = 32$ and $k = 0$ for the Stokes problem with $\nu = 1$. Numerical solutions corresponding to different algorithms are plotted in Figure 1. The left panel plots the numerical solution for first component of velocity, the middle panel plots the numerical solution for second component of velocity, and the right panels plots the numerical solution for pressure. As shown in this figure, the numerical solution in velocity is nothing like zero although one can still observe convergence rate for the problem, which is $\mathcal{O}(h^{k+1})$ for $|||\mathbf{Q}_h\mathbf{u} - \mathbf{u}_h|||$ and $\mathcal{O}(h^{k+2})$ for $\|\mathbf{Q}_0\mathbf{u} - \mathbf{u}_0\|$. In contrast, the magnitude for velocity produced by Algorithm 2.2 is around 10^{-15}. As the above discussions, this validates our predictions.

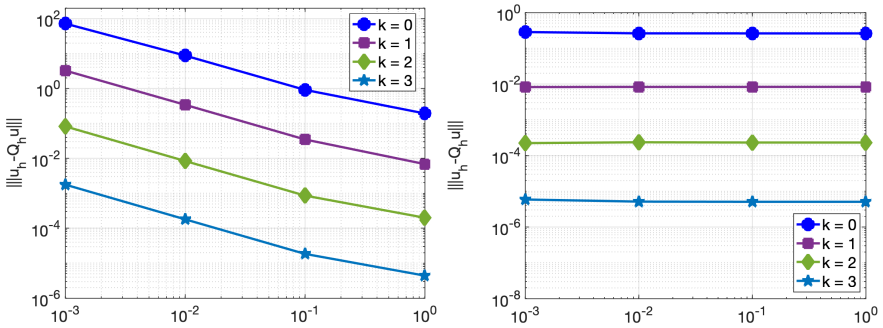

FIGURE 2. Example 4.2: Error profiles and convergence results for $|||\cdot|||$-norm on triangular mesh: standard scheme Algorithm 2.2 (left); new scheme Algorithm 2.1 (right).

4.2. **Test 2.** In this second test, we shall consider the convergence results with respect to viscosity ν. Let $\Omega = (0,1)^2$, and the source term $\mathbf{f}$ and boundary conditions are chosen such that exact solutions are chosen as follows:

$$\mathbf{u} = \begin{pmatrix} \sin(\pi x)\sin(\pi y) \\ \cos(\pi x)\cos(\pi y) \end{pmatrix},\ p = 2\cos(\pi x)\sin(\pi y).$$

We perform two numerical schemes for different values in ν and $h = 1/N$ with $N = 16$ for weak Galerkin finite element $k = 0, 1, 2, 3$. Let $\nu = 10^{-3}, 10^{-2}, 10^{-1}, 1$ and error profiles and the convergence results are plotted in Figure 2-Figure 4. Our observations are described as following.

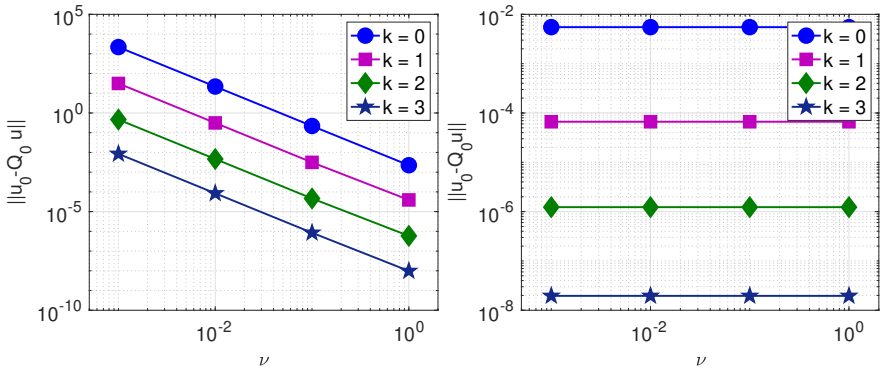

FIGURE 3. Example 4.2: Error profiles and convergence results for L^2-norm on triangular mesh: standard scheme Algorithm 2.2 (left); new scheme Algorithm 2.1 (right).

Figure 2 illustrates the performance for Algorithm 2.1 (right panel) and Algorithm 2.2 (left panel) for the simulation in velocity measured in $|||\cdot|||$-norm with respect to viscosity coefficient ν. As one can see from this comparison that WG 2 will produce a solution for velocity depending on the viscosity coefficient ν. As decreasing values in ν, the energy norm for velocity is increasing. Furthermore, if ν is too small, the energy norm will be unbounded. This observation validates the convergence results as $|||\mathbf{u}_h - \mathbf{Q}_h\mathbf{u}||| \leq Ch^{k+1}(\|\mathbf{u}\|_{k+2} + \nu^{-1}\|p\|_{k+1})$. Different as Algorithm 2.2, Algorithm 2.1 shows the robustness with respect to ν. When we reducing the values in ν, in fact, the velocity error measured in H^1-like norm keeps almost the same. It shows the effectivity of our proposed numerical scheme.

The left and right panels in Figure 3 compare the behavior of velocity simulation by Algorithm 2.2 (left panel) and Algorithm 2.1 (right panel). We have the similar observation as above: Algorithm 2.1 delivers a viscosity robust simulation, while the simulation of velocity through Algorithm 2.2 shows the relations depending on viscosity.

The third experiment in this second is the validation in simulation of pressure and the numerical profiles are shown in Figure 4. Left figure plots the performance for Algorithm 2.2 and right figure plots the profiles for Algorithm 2.1. For this test, Algorithm 2.2 shows the similar in-dependency with respect to viscosity. However, the Algorithm 2.1 produce a better results for pressure as reducing values in ν. This is because of the convergence conclusions as $\|\Pi_h p - p_h^{\mathrm{WG}_2}\| \leq Ch^{k+1}(\nu\|\mathbf{u}\|_{k+2} + \|p\|_{k+1})$, but $\|\Pi_h p - p_h^{\mathrm{WG}_1}\| \leq C\nu h^{k+1}\|\mathbf{u}\|_{k+2}$. All these observations confirm our theoretical proof.

4.3. **Test 3.** In this test, we shall consider the variable viscosity test. Let $\Omega = (0,1)^2$ and viscosity is described as

$$\begin{aligned}\text{Case 1: } \nu &= \nu_{\min} + (\nu_{\max} - \nu_{\min})e^{-10^{13}((x-0.5)^{10}+(y-0.5)^{10})},\\ \text{Case 2: } \nu &= \nu_{\min} + (\nu_{\max} - \nu_{\min})(1 - e^{-10^{13}((x-0.5)^{10}+(y-0.5)^{10})}).\end{aligned}$$

Source function $\mathbf{f}$ and the boundary conditions are chosen to match the equation such that the exact solutions are as follows:

$$\mathbf{u} = \begin{pmatrix} 3000x^2(1-x)^4y^2(1-y)^2 - 2000x^2(1-x)^4y^3(1-y) \\ -2000x(1-x)^4y^3(1-y)^2 + 4000x^2(1-x)^3y^3(1-y)^2 \end{pmatrix},$$

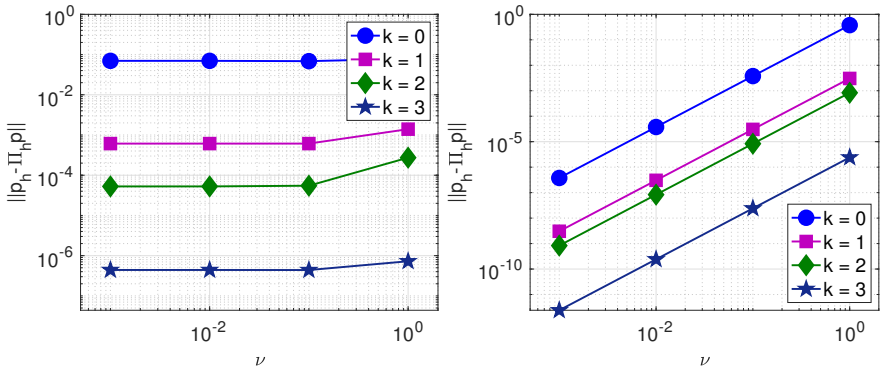

FIGURE 4. Example 4.2: Error profiles and convergence results for $\|p-p_h\|$ on triangular mesh: standard scheme Algorithm 2.2 (left); new scheme Algorithm 2.1 (right).

$$p = \pi^2(xy^2\cos(2\pi x^2 y) - x^2 y\sin(2\pi xy)) + 1/8.$$

In this test, we shall choose $\nu_{\min} = 1E-5$ and $\nu_{\max} = 1$ for testing. The profiles for viscosity ν are plotted in Figure 5 for Case 1 and Case 2.

Algorithm 2.1 and 2.2 for $k = 0$ are performed on the mesh with $h = 1/80$, and the numerical solution for velocity are illustrated in the middle and right panels of Figure 5. The exact solution is very similar as the numerical solutions produced by Algorithm 2.1, so here we omit the plot of exact solutions. However, one can observe significant difference between numerical solutions by Algorithm 2.2 and exact solutions. This test again validates that our new algorithm is a robust numerical scheme with respect to viscosity coefficient.

4.4. **Test 4.** (Three-dimensional problem). Let $\Omega = (0,1)^3$, $\mathbf{u} = (u_1, u_2, u_3)$ with

$$\begin{aligned} u_1 &= 1/2\sin(2\pi x)\cos(2\pi y)\cos(2\pi z) \\ u_2 &= 1/2\cos(2\pi x)\sin(2\pi y)\cos(2\pi z) \\ u_3 &= -\cos(2\pi x)\cos(2\pi y)\sin(2\pi z) \\ p &= \sin(2\pi x)\sin(2\pi y)\sin(2\pi z). \end{aligned}$$

In this experiment, we shall apply Algorithm 2.1 and 2.2 to three-dimensional problems on the tetrahedral mesh. The size of mesh is denoted as h and we test the performance of lowest order weak Galerkin element with $k = 0$. The numerical performance and convergence test are summarized in Table 1. Optimal convergence rates can be obtained in this table for velocity error measured in $|||\cdot|||$-norm and $\|\cdot\|$-norm; for pressure error measured in L^2-norm by Algorithm 2.1. Although in the simulation of Algorithm 2.2, we can still observe desired convergence rate, the magnitude of errors is much bigger than that of Algorithm 2.1. Besides, as reducing values in ν, the error of pressure by Algorithm 2.1 is decreased. The above conclusions again validate our theoretical conclusions.

5. **Conclusion and remark.** In this paper, we considered the pressure robust scheme for Stokes equations based on the weak Galerkin finite element framework. The scheme has the same stiffness matrix as the previous weak Galerkin scheme but only varies at the right hand side assembling. The numerical analysis demonstrates

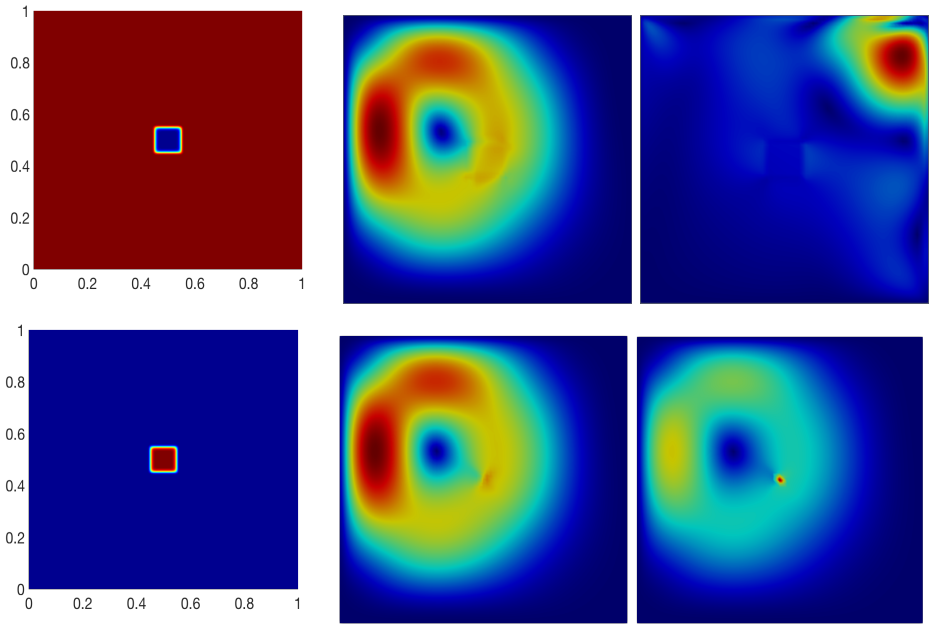

FIGURE 5. Example 4.3: Profile for viscosity (left); magnitude plot for velocity by Algorithm 2.1 (middle); magnitude plot for Algorithm 2.2 (right). Top row illustrates the results for Test Case 1; Bottom row illustrates the results for Test Case 2.

TABLE 1. Example 4.4: Numerical results and convergence test for $k = 0$.

	Algorithm 2.1						Algorithm 2.2					
$1/h$	$\|\|\|\mathbf{e}_h\|\|\|$	Rate	$\|\|\mathbf{e}_h\|\|$	Rate	$\|\|\epsilon_h\|\|$	Rate	$\|\|\|\mathbf{e}_h\|\|\|$	Rate	$\|\|\mathbf{e}_h\|\|$	Rate	$\|\|\epsilon_h\|\|$	Rate
	$\nu = 1$											
2	2.69E+2		7.22		1.11E+2		2.69E+2		7.22E		1.11E+2	
4	2.35E+2	0.2	3.46	1.1	5.70E+1	1.0	2.35E+2	0.2	3.46	1.1	5.70E+1	1.0
8	1.54E+2	0.6	1.14	1.6	2.81E+1	1.0	1.54E+2	0.6	1.14	1.60	2.81E+1	1.0
16	7.65E+1	1.0	2.95E-1	2.0	1.31E+1	1.1	7.65E+1	1.0	2.95E-1	2.0	1.31E+1	1.1
32	3.83E+1	1.0	7.39E-2	2.0	6.55	1.0	3.83E+1	1.0	7.38E-2	2.0	6.55	1.0
	$\nu = 1e-2$											
2	2.69E+2		7.22		1.19		2.75E+2		7.74		1.12	
4	2.35E+2	0.2	3.46	1.1	5.77E-1	1.1	2.35E+2	0.2	3.46	1.2	5.70E-1	1.0
8	1.54E+2	0.6	1.14	1.6	2.81E-1	1.0	1.68E+2	0.5	1.27	1.5	2.88E-1	1.0
16	7.65E+1	1.0	2.95E-1	2.0	1.30E-1	1.1	7.86E+1	1.1	3.06E-1	2.1	1.33E-1	1.1
32	3.83E+1	1.0	7.38E-2	2.0	6.50E-2	1.0	3.93E+1	1.0	7.65E-2	2.0	6.65E-2	1.0
	$\nu = 1e-4$											
2	2.69E+2		7.22		1.19E-2		8.92E+3		3.16E+2		1.25E-1	
4	2.35E+2	0.2	3.46	1.1	5.77E-3	1.1	5.34E+3	0.7	9.40E+1	1.8	7.15E-2	0.8
8	1.54E+2	0.6	1.14	1.6	2.81E-3	1.0	4.29E+3	0.3	3.53E+1	1.4	4.53E-2	0.7
16	7.65E+1	1.0	2.95E-1	2.0	1.30E-3	1.1	2.11E+3	1.0	9.11	2.0	1.62E-2	1.5
32	3.83E+1	1.0	7.38E-2	2.0	6.50E-4	1.0	1.06E+3	1.0	2.28	2.0	8.10E-3	1.0

that the error of velocity is independent of error in pressure and thus shows the robustness with respect to viscosity parameters.

As the future work, we shall consider developing robust schemes for Brinkmann equations and Navier-Stokes equations.

REFERENCES

[1] C. Brennecke, A. Linke, C. Merdon and J. Schöberl, Optimal and pressure-independent L^2 velocity error estimates for a modified Crouzeix-Raviart Stokes element with BDM reconstructions, *J. Comput. Math.*, **33** (2015), 191–208.

[2] D. A. Di Pietro, A. Ern, A. Linke and F. Schieweck, A discontinuous skeletal method for the viscosity-dependent Stokes problem, *Comput. Methods Appl. Mech. Engrg.*, **306** (2016), 175–195.

[3] J. Guzmán and M. Neilan, Conforming and divergence-free Stokes elements on general triangular meshes, *Math. Comp.*, **83** (2014), 15–36.

[4] C. Lehrenfeld and J. Schöberl, High order exactly divergence-free hybrid discontinuous Galerkin methods for unsteady incompressible flows, *Comput. Methods Appl. Mech. Engrg.*, **307** (2016), 339–361.

[5] A. Linke, A divergence-free velocity reconstruction for incompressible flows, *C. R. Math. Acad. Sci. Paris*, **350** (2012), 837–840.

[6] A. Linke, On the role of the Helmholtz decomposition in mixed methods for incompressible flows and a new variational crime, *Comput. Methods Appl. Mech. Engrg.*, **268** (2014), 782–800.

[7] A. Linke, G. Matthies and L. Tobiska, Robust arbitrary order mixed finite element methods for the incompressible Stokes equations with pressure independent velocity errors, *ESAIM Math. Model. Numer. Anal.*, **50** (2016), 289–309.

[8] Y. Liu and J. Wang, Simplified weak Galerkin and new finite difference schemes for the Stokes equation, *J. Comput. Appl. Math.*, **361** (2019), 176–206.

[9] L. Mu, J. Wang, Y. Wang and X. Ye, A weak Galerkin mixed finite element method for biharmonic equations, in *Numerical Solution of Partial Differential Equations: Theory, Algorithms, and Their Applications*, Springer Proc. Math. Stat., 45, Springer, New York, 2013, 247–277.

[10] L. Mu, J. Wang and X. Ye, Effective implementation of the weak Galerkin finite element methods for the biharmonic equation, *Comput. Math. Appl.*, **74** (2017), 1215–1222.

[11] T. Tian, Q. Zhai and R. Zhang, A new modified weak Galerkin finite element scheme for solving the stationary Stokes equations, *J. Comput. Appl. Math.*, **329** (2018), 268–279.

[12] J. Wang and X. Ye, A weak Galerkin finite element method for second-order elliptic problems, *J. Comput. Appl. Math.*, **241** (2013), 103–115.

[13] J. Wang and X. Ye, A weak Galerkin finite element method for the Stokes equations, *Adv. Comput. Math.*, **42** (2016), 155–174.

[14] S. Zhang, A new family of stable mixed finite elements for the 3D Stokes equations, *Math. Comp.*, **74** (2005), 543–554.

Received April 2020; revised July 2020.

E-mail address: binwang.0213@gmail.com
E-mail address: linmu@uga.edu